ACS Sustainable Chemistry & Engineering

Research Article

pubs.acs.org/journal/ascecg

Biowaste Sago Bark Based Catalyst Free Carbon Nanospheres: Waste to Wealth Approach

Gurumurthy Hegde,*[,†] Shoriya Aruni Abdul Manaf,[‡] Anuj Kumar,[§] Gomaa A. M. Ali,[‡] Kwok Feng Chong,[‡] Zainab Ngaini,[∥] and K. V. Sharma[⊥]

[†]BMS R & D Centre, BMS College of Engineering, Basavanagudi, Bangalore, 560019, India

[‡]Faculty of Industrial Sciences & Technology, Universiti Malaysia Pahang, 26300, Gambang, Kuantan, Malaysia

[§]Czech Technical University in Prague, Faculty of Civil Engineering, Department of Building Structures, Thákurova 7, 166 29 Praha 6 - Dejvice, Czech Republic

[∥]Department of Chemistry, Faculty of Resource Science and Technology, Universiti Malaysia Sarawak, 94300, Sarawak, Malaysia

[⊥]Department of Mechanical Engineering, University Technology Petronas, Bandar Seri Iskandar, 31750, Tronah, Perak, Malaysia

Supporting Information

ABSTRACT: Catalyst-free carbon nanospheres were synthesized using simple one-step pyrolysis techniques where biowaste sago bark is used as a carbon precursor. Obtained carbon nanospheres showed a porous nature and revealed that more than 95% carbon is present in the synthesized carbon nanospheres with particle size ranging from 40 to 70 nm. An electrochemical study showed a specific capacitance value of 180 F g^{-1} at 2 mV s^{-1} and the cycling stability up to 1700 cycles. Obtained carbon nanospheres are useful in supercapacitor applications. The presented study revealed a waste to wealth approach thereby reducing waste in the environment.

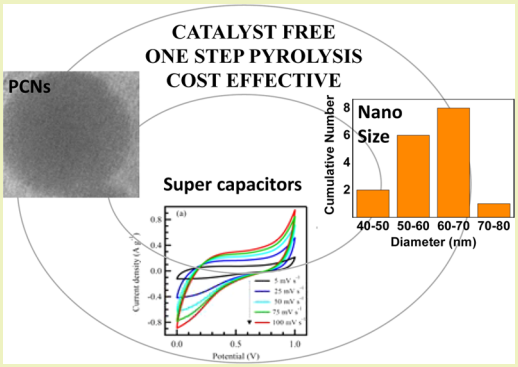

KEYWORDS: *Sago bark, Nanoporous carbon, Pyrolysis, Supercapacitors, Waste to wealth*

INTRODUCTION

Carbon-based nanomaterials have promising applications in nanoelectronics,[1] microelectrical devices,[2] electrochemistry,[3,4] sensors,[5] catalysis,[6] and ultracapacitors.[7−9] Among different forms of carbon nanomaterials,[10−13] carbon nanospheres are gaining interest because, in its spherical arrangement, they are normally unclosed shells with rather waving flakes that follow the curvature of the sphere. This forms many open edges at the surface creating reactive "dangling bonds," which provides the spheres with high chemical activity, establishing them as good candidates for their use in various applications.[11]

Various methods have been reported for the synthesis of carbon nanosphere transition and/or rare earth metal oxides as catalysts[14] and carbon nanospheres from the carbonization of polyethylene−poly(vinyl chloride) in a sealed gold tube under a pressure of 30 MPa,[15] in carbon vapor from the decomposition of β-SiC powder,[16] etc. Carbon nanospheres of 20−500 μm are found as a side product in the synthesis of fullerene by the deposition of gaseous carbon.[17] Arc discharge and laser ablation methods have also been used for the synthesis of structured carbon.[18,19] Although the catalytically assisted chemical vapor deposition method has emerged as a promising technique,[20] an economically viable method for the preparation of a bulk quantity of carbon nanospheres under reasonable experimental conditions is still lacking to date. Many methods use petroleum products as a source for carbon material preparation, which has a negative environmental impact, and also these methods suffer from many problems such as the production of a significant quantity of undesired byproducts, additional purification steps, low yields and high energy requirements, high cost production, etc. Thus, the need for alternate carbon sources for the synthesis of environmentally friendly, cost-effective carbonaceous materials is the present day's requirement.

On the other hand, carbon materials with a high degree of porosity and high specific surface area are employed in the development of advanced energy storage systems such as electrochemical capacitors.[21−25] An electrical/electrochemical double layer capacitor (EDLC), also known as a "supercapacitor" or "ultracapacitor," is a promising one, which is characterized by energy density in the range of 1−10 W h kg and a power density of 1−10 kW kg. These high parameters influence the replacement of the batteries as storage media by EDLC in many systems where traditional batteries are used (e.g., hybrid electric vehicles, power back-up systems, UPS,

Received: June 10, 2015
Revised: July 27, 2015
Published: July 28, 2015

DOI: 10.1021/acssuschemeng.5b00517
ACS Sustainable Chem. Eng. 2015, 3, 2247−2253

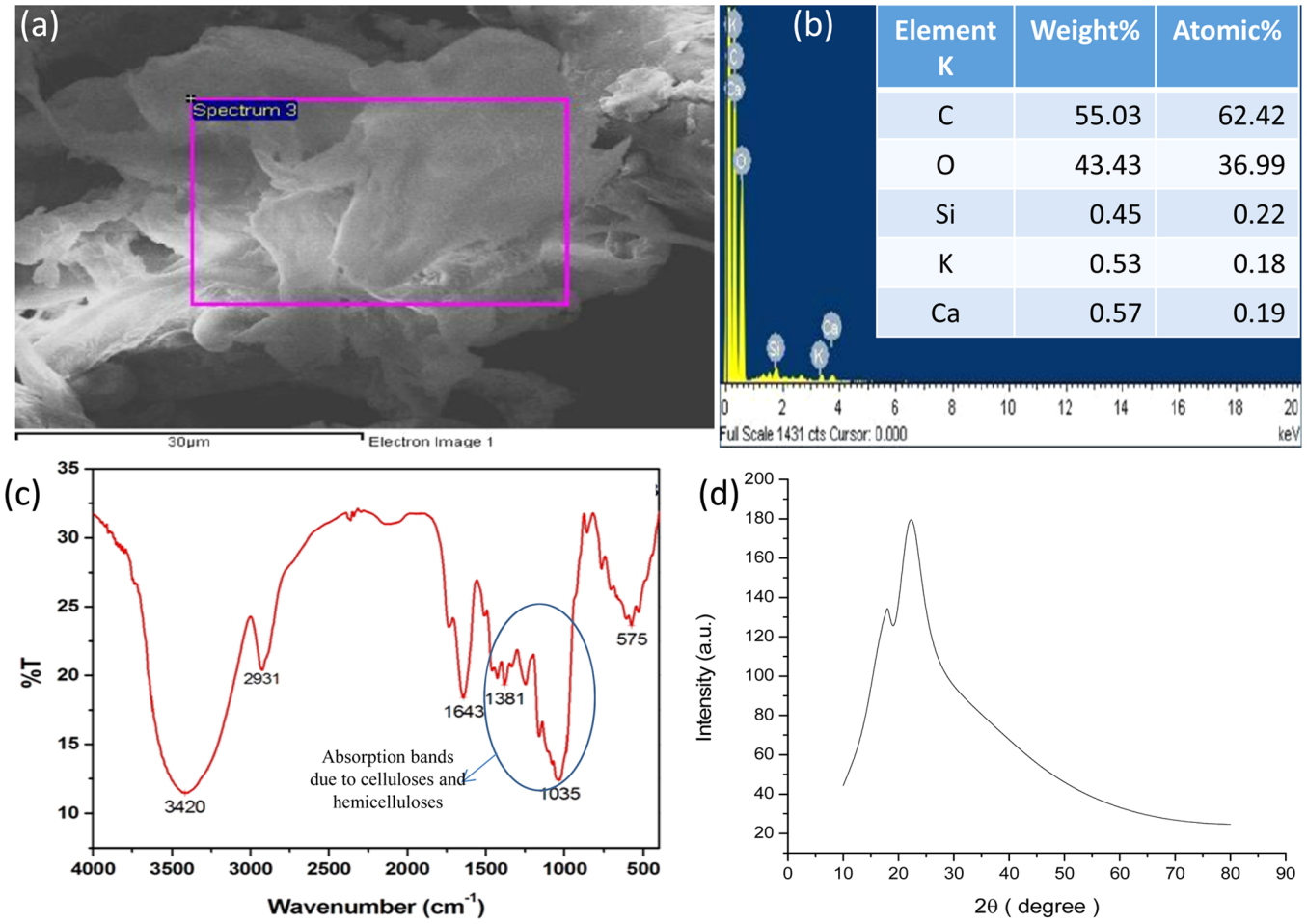

Figure 1. (a) FESEM image of raw sago bark and (b) EDX spectrum taken from the square area in part a. (c) FT-IR spectrum and (d) wide-angle XRD pattern of raw sago bark.

etc.). Very recently, we came up with an alternate source for the fabrication of carbonaceous material and reported the porous carbon nanoparticles and its electrochemical applications.[26−28] Apart from this, direct laser writing of microsupercapacitors on hydrated graphite oxide films were also reported as excellent materials for supercapacitors.[29]

In our continued investigation, herein we report the synthesis of carbon nanospheres (CNSs) by a catalyst-free pyrolysis technique from biowaste sago bark, which is an inexpensive fibrous residue obtained from the sago palm tree. The prepared CNSs are characterized using various characterization techniques to prove its spherical shape and also for its ability to be used as potential materials for super capacitor applications. The advantage of the presented method is that the described process can be applied in bulk synthesis, and also it is environment friendly. It is also a bold step to turn waste materials into useful producst by utilizing the waste to wealth concept.

RESULTS AND DISCUSSION

Sago bark is the waste solid residue resulted from sago starch processing industries. Because of its cellulosic−hemicellulose and lignin content, sago bark can be used for sustainable development: biowaste to wealth management. Thus, in the present work, sago bark is used as a raw material for the production of carbon nanospheres (CNSs) by a simple environmentally benign pyrolysis technique. This technique yielded CNSs of highly ordered ultrasmall sized nanospheres of carbon.

Sago bark was subjected to TGA analysis to set the pyrolysis temperature (Figure S1-s1). In the TGA curve of sago bark, the carbonization peak appearing around 80−90 °C is due to the decomposition of the lattice held water of sago bark. The main carbonization peak in the range of 200−450 °C centered at 320 °C with a maximum weight loss (i.e., 70%) can be attributed to the decomposition of cellulose and lignin contents, and another carbonization peak around 900 °C may be due to the presence of metal oxide traces. The FESEM-EDX results also accounted for the high carbon content in sago bark (Figure 1a and b). Figure S1-s2 shows the stability of the CNSs after pyrolysis at 500 °C. One can see the stability over a wide temperature range showing complete carbonization.

FTIR analysis was helpful in elucidating the functional groups of the sago bark. According to Sun et al., the cellulose fraction of sago bark consisted of xylose and glucose as the major components of the isolated hemicelluloses and small amounts of other sugars together with noticeable amounts of arabinose and galactose.[30] Lignin, on the other hand, influences the structural rigidity by stiffening and holding the fibers together. In the FTIR spectrum (Figure 1c), the characteristic absorption bands observed around 1160 and 1420 cm^{-1} can be assigned to hemicelluloses and cellulose, respectively. This may be ascribed to glycosidic linkage C−O−C. The strong stretching vibration band observed around 1643 cm^{-1} can be

DOI: 10.1021/acssuschemeng.5b00517
ACS Sustainable Chem. Eng. 2015, 3, 2247−2253

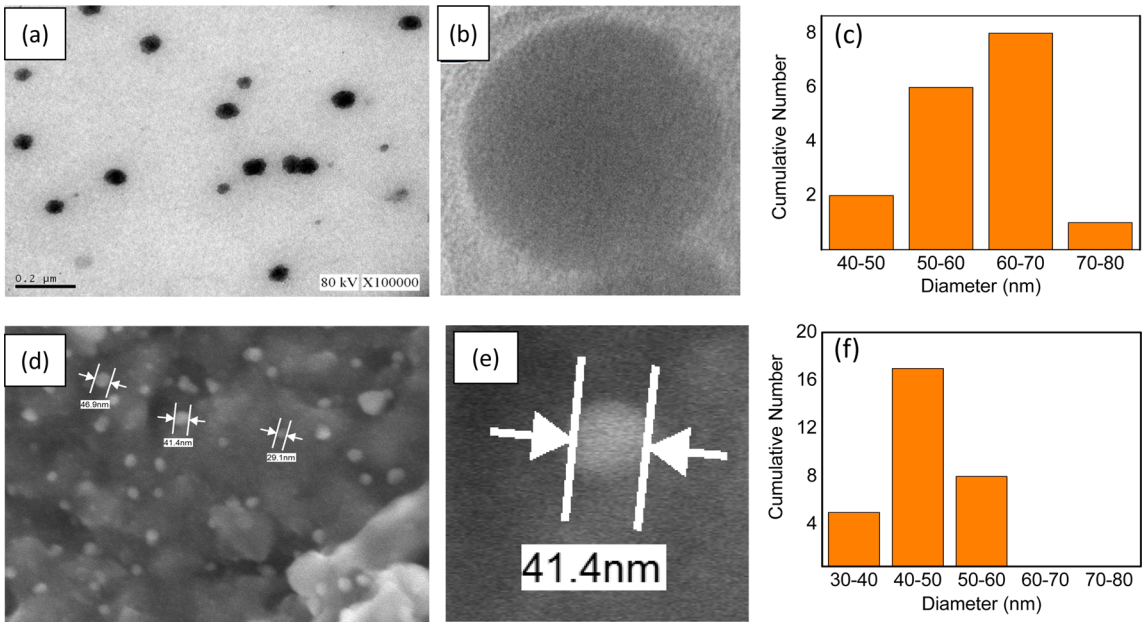

Figure 2. (a,b) TEM image, (c) the particle size distribution histogram for CNSs for TEM, (d,e) FESEM image for CNSs, and (f) the particle size distribution histogram for CNSs for FESEM. The curve in parts c and f shows the average particle size.

assigned to a carbonyl group (C═O), which gives evidence of the high carbon content of sago bark.[31,32] Along with this, the other numerous absorption bands due to the structural diversity of celluloses and hemicelluloses,[33] which includes C−OH, C−H, and −C−C−O functional groups, were observed in the region 2931 and 1500−900 cm^{-1}. The bands at 1160 and 1035 cm^{-1} suggest the presence of arabinosyl residues and α-glucan of hemicelluloses.[34] The absorption peak at 575 cm^{-1} might appear due to the presence of some oxide particle accumulations in sago bark. Hence, the observed results are in accordance with the literature record. Thus, the fibrous residue with a coarse nature may act as the inbuilt template for the formation of the nanospheres.

The XRD spectrum of sago bark exhibited two peaks which are related to the microcrystalline nature of the cellulose.[35] The first peak at 2θ = 17.74° corresponds to (1 1 0) and the second at 2θ = 22.09° corresponds to the (1 2 0) plane (Figure 1d). Thus, as is evident from the EDX analysis, FTIR and XRD studies also highlight the high content of carbon in sago bark. These observations prompted us to fabricate nanoparticles at a pyrolysis temperature of 500 °C which contributed to the formation of highly ordered CNSs. These temperatures are not optimum but good enough to show the potentiality of the materials. More study is in progress to check the higher temperature effects in these directions.

The raw sago bark particles were pyrolyzed in tube furnace at 500 °C for 2 h under the continuous flow of N_2. Finally, the pyrolized products were washed with HCl solution and then with deionized water. TEM revealed the formation of uniformly distributed sphere shaped carbon nanoparticles at a 500 °C pyrolysis temperature (Figure 2a,b). One can see the high porous nature of the CNSs when it is zoomed (Figure 2b). The average particle size is 65 ± 5 nm as obtained from the histogram (Figure 2c). The FESEM images (Figure 2d,e) also exhibited a similar shape for the carbon nanoparticles, also the magnified image of CNSs confirm this porous structure formation (Figure 2e). The wide distributions of the nanoparticles (~50 nm) were observed in histogram of the FESEM images (Figure 2f). The energy dispersive X-ray (EDX) analysis showed a very high percentage content of carbon using biowaste materials (~95% atomic percentage) in the prepared nanospheres (Figure S1-s3). The TEM and FESEM results suggest the conversion of biowaste raw sago bark into carbon nanoparticles with uniform particle size possessing high carbon content belonging to the class of carbon nanospheres (CNSs) by a facile catalyst free pyrolysis technique. This was further ascertained by FTIR analysis of CNSs (Figure S1-s4). A large deviation in the bands of lignocelluloses in the region 1500−900 cm^{-1} was observed in CNSs' FTIR spectrum. This may be due to the conversion of the fibrous residue of sago bark into carbon nanospheres. The strong absorption band around 1635 cm^{-1} was assigned to the C═O bond of the carbonyl group. The absorption bands around 3457 and 2900 cm^{-1} are assigned to the C−OH and C−H stretching modes of the carbon skeleton.

The porous nature was investigated by the Brunauer−Emmett−Teller (BET) method. In IUPAC classification, the pores with diameters less than 2 nm are classified as micropores, whereas the pores with diameters from 2 to 50 nm are classified as mesopores. For the CNSs treated at 500 °C, the BET surface area (S_{BET}) is 58 $m^2 \cdot g^{-1}$, and the t-plot micropore surface area (St-plot) is 32 $m^2 \cdot g^{-1}$. The $S_{t\text{-plot}}/S_{BET}$ value is quite high (55.2%), meaning large contribution from the micropores. Hence, the fabricated CNSs exhibited a good microporous structure. Figure 3 shows the nitrogen soprtion curve and pore distribution of CNSs.

X-ray analysis showed that the CNSs possess crystalline and graphitic characteristics with prominent (0 0 2) and (1 0 1) planes. The CNSs exhibited a main diffraction peak at 2θ = 26.96° corresponding to the (0 0 2) plane which can be attributed to graphite-2H (ICDD 411487) as shown in Figure 4a. Quantitative measurement of graphitic character, the interlayer d spacing d_{002} is 3.5005 Å.[36] The XRD spectrum showed a peak at 2θ = 43.98° with interlayer d spacing of 2.064 Å, which can be assigned to (1 0 1) lattice planes of graphite.[37] Very surprisingly, CNSs exhibited a very small (almost

DOI: 10.1021/acssuschemeng.5b00517
ACS Sustainable Chem. Eng. 2015, 3, 2247−2253

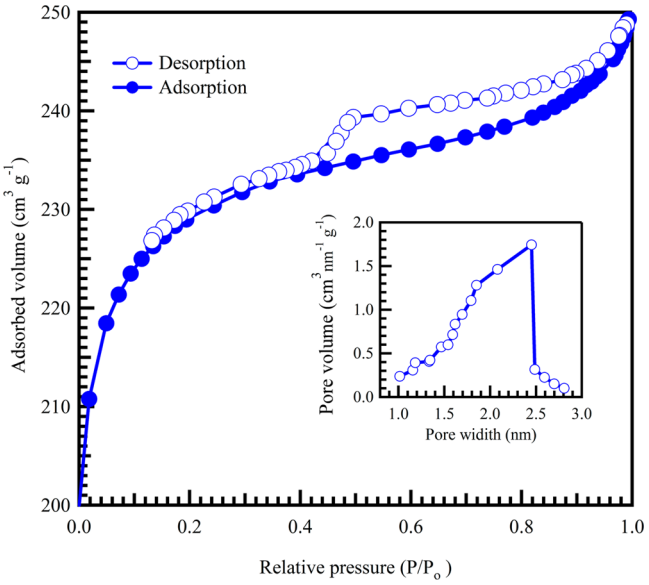

Figure 3. Adsorption and desorption curve of liquid nitrogen during BET analysis of CNSs and BJH pore distribution in prepared CNSs.

negligible) peak at 2θ = 21.0339° with d_{002} = 4.2201 Å. This peak may have arisen from the highly crystalline cellulose fibers, i.e., hemicelluloses and celluloses of sago bark.[35,38,39] Thus, the XRD analysis suggests the evolution of a new class of carbon nanomaterial with high graphitic nature of the CNSs.

Raman spectroscopy is extremely useful in deducing the graphitic characteristic of carbon nanomaterial. The carbon materials present two main peaks: diagnostic of disorder in the carbon structure denoted as D- and the diagnostic of structural order denoted as G- bands. In the present CNSs, obtained at a pyrolysis temperature of 500 °C (Figure 4b), the D- band was observed at 1346 cm^{-1}. The CNSs exhibited a G- band at 1593 cm^{-1}, which is related to the sp^2 bonded carbon atom from stretching modes of C═C bonds corresponding to the E_{2g} mode of graphite.[40,41] The graphitic character can further be assessed by the relative intensities of D- and G- bands (I_D/I_G) and full-width at half-maximum (fwhm) of the G- band. In present case, the I_D/I_G ratio was found to be 0.84,[42] and fwhm of the G- band is found to be 62 cm^{-1}. Apart from this, we observed two peaks at 2781 and 3152 cm^{-1} which can be assigned to the second order D (2 × D) and G (2 × G) modes, respectively,[43] and they are very weak compared to the D- and G- bands. Thus, Raman results together with XRD analysis gives evidence for the strong graphitic character of the prepared CNSs.

The ζ potential is often used as an index of the magnitude of electrostatic interaction between colloidal particles and is thus a measure of the colloidal stability of the solution. The measured distributions are generally broad and asymmetric due to the range of nanosizes, and the distributions can clearly be nonionic. We estimated the ζ potential of the CNSs to be the center of the distribution with the ζ potential 0 to −40 mV with a peak value of −29.5 mV, as shown in Figure 5 (phase plot is given in Figure S1-s5). So, the prepared carbon nanoparticles are stable from electrostatic considerations.[44]

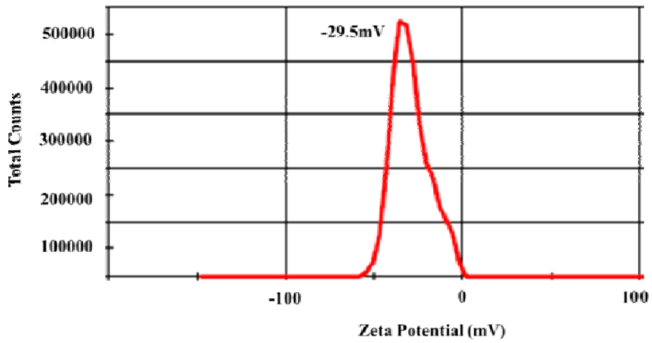

Figure 5. Zeta potential curve for aqueous solution of CNSs treated at 500 °C.

Due to the ever-growing populations, it is required to find a new solution for the energy demands. Supercapacitors are the ideal candidates for fulfilling energy demands to some extent. Carbon nanoparticles played a vital role to handle these responsibilities. With respect to that, electrochemical properties of CNSs are presented in Figures 6 and 7. CNSs show capacitive behavior as corroborated by CV curves measured at different scan rates which exhibit an almost rectangular-like shape as shown in Figure 6a. The specific capacitance (Cs) values were calculated by integrating the area under the curve. The present CNSs show a Cs of 180 F g^{-1} at 2 mV s^{-1}, and it is observed that the values decrease with increasing scan rate (Figure 6b).

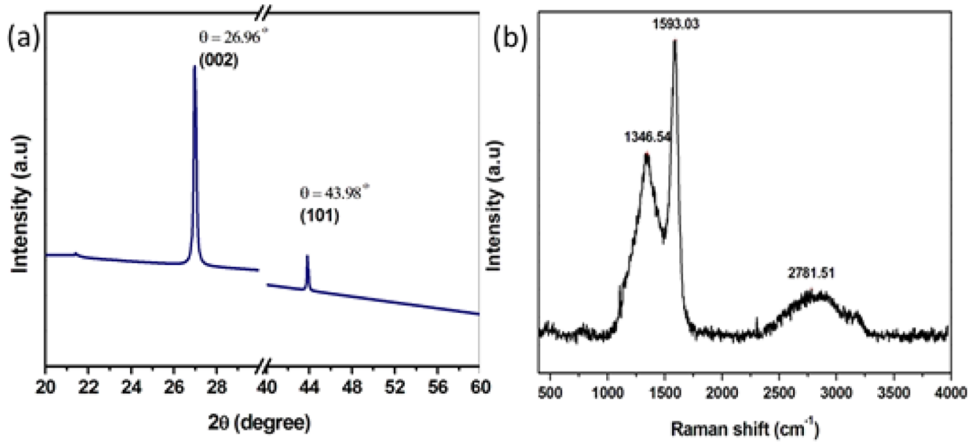

Figure 4. (a) Wide angle XRD pattern and (b) Raman spectrum of CNSs.

DOI: 10.1021/acssuschemeng.5b00517
ACS Sustainable Chem. Eng. 2015, 3, 2247−2253

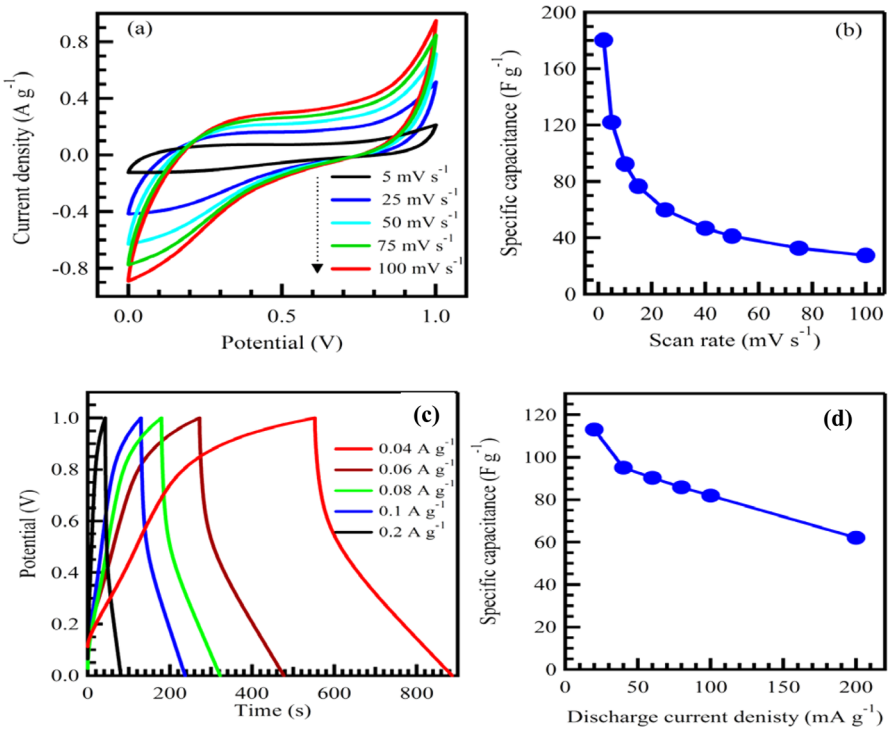

Figure 6. Electrochemical properties of CNSs: Cyclic voltammetry curves (a) at different scan rates and specific capacitance (b) as a function of scan rate. Galvanostatic charge−discharge curves (c) at different current densities and specific capacitance (d) as a function of current density.

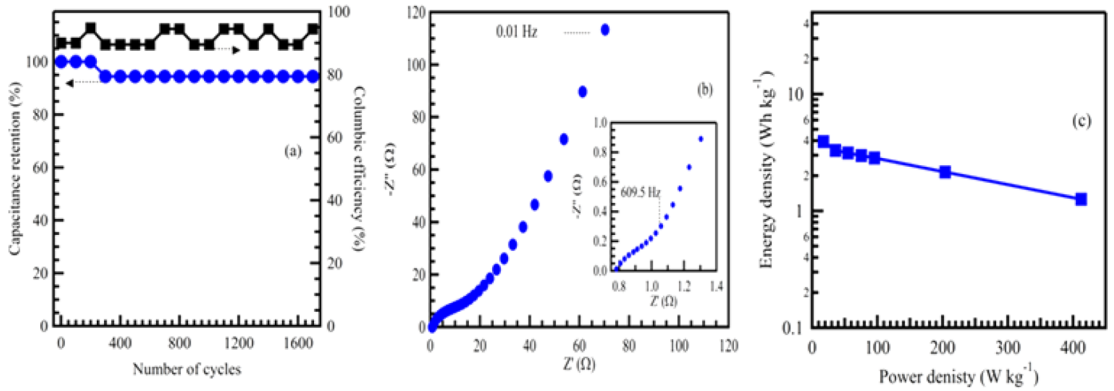

Figure 7. Electrochemical properties of CNSs showing (a) cycle life stability curve (left vs bottom) and coulumbic efficiency (right vs bottom) at 0.2 Ag^{1-} current density; (b) Nyquist plots; inset, a zoomed view of Nyquist plots in the high-frequency region; (c) Ragone plot.

Figure 5c presents the charge−discharge tests at different current densities. The plot indicates rapid current−voltage response. Moreover, CNSs show a high Cs value of 113 F g^{-1} at 20 mA g^{-1} and decrease with increasing discharge current (Figure 6d). The cycling stability of CNSs was studied using galvanostatic charge−discharge at 0.2 A g^{-1} for 1700 cycles as presented in Figure 7a. The results show that the cycling stability still maintained more than 94% of its original capacitance even after 1700 cycles, indicating excellent cyclic stability. CNSs also showed a high columbic efficiency of 95%, as shown in Figure 7a. Such high capacitance retention of up to 1700 cycles suggests that the CNSs are a good candidate for supercapacitor applications.

The electrochemical impedance spectroscopy (EIS) study was carried to further investigate the electrochemical properties for CNSs. A Nyquist plot for CNSs is shown in Figure 7b. The inset of Figure 7b represents the high frequency region of the recorded full impedance plot. A small semicircle in the high frequency region and a vertically straight line in the low frequency region can be seen. The solution resistance (R_s) was found to be very small (0.78 Ω), indicating high electrical conductivity of CNSs. The charge transfer resistance (R_{ct}) associated with the surface electrode properties was found to be 0.26 Ω. A detailed investigation in this direction is in progress to enhance the specific capacitance value by activating the carbon nanospheres and will be reported elsewhere. The Ragone plot for sago-bark-based carbon nanospheres is shown in Figure 7c, presenting the maximum energy density of 5 W h kg^{-1} and maximum power density of 400 W kg^{-1}. The energy and power densities were calculated using the equation reported elsewhere.[45] The energy density was found to be reasonable in comparison with those obtained for activated carbon.[46] The obtained high values of supercapacitance may be due to the porous nature of carbon and high surface area. We are now in the process of activating the carbon, thereby

DOI: 10.1021/acssuschemeng.5b00517
ACS Sustainable Chem. Eng. 2015, 3, 2247−2253

increasing the surface area so that one can get much superior super capacitors; this will be published elsewhere.

CONCLUSION

In conclusion, simple, cost-effective carbon nanospheres obtained from waste sago bark without the addition of any catalyst were synthesized. Obtained CNSs show high quality particles with uniform sizes ranging from 40 to 70 nm along with the ability to bulk produce. Due to their porous nature, they do show reasonable specific capacitance for the application of super capacitors. This is a bold step to convert biowaste materials into useful products, thereby reducing pollution in the environment.

EXPERIMENTAL SECTION

Synthesis and Purification of CNSs. The dry sago bark was obtained from a sago palm estate in Malaysia where major sago related products were being made and also a heavy amount of waste produced from sago bark. The fibrous residue was separated and dried in an oven at 110 °C for 2 days to remove all the moisture. The dry sago bark was crushed, followed by grinding at 12 000 rpm using a grinder (Retsch, ZM 200, Germany), and further, the ground raw sago bark was sieved to a particle size of ∼60−70 μm. Then, the raw sago bark was pyrolyzed in a tube furnace (Nabertherm, EW-33334-36) at 500 °C for 2 h under a continuous flow of nitrogen (N_2) (150 mlcm^{-3}) at a heating rate of 5 °C m^{-1} and simultaneously cooled down to room temperature in a N_2 atmosphere to get a pyrolyzed product. The pyrolized products were washed with 1 M hydrochloric acid (HCl) and then with deionized water to get pure CNSs.

Characterization of CNSs. The raw sago bark and CNSs were characterized using FTIR (Perkin, Elmer Spectrum 100), FESEM-EDX (JEOL, JSM-7800F), XRD (Rigaku Mineflex II), TEM (JEOL, JSM 1230), and Themogravimetric Analysis (TGA; Mettler Toledo TGA/DSC HT/1600). The BET surface area and pore width of CNSs were evaluated using a Micromeritics ASAP 2020 under a low pressure dose; the CNSs samples was degassed for 12 h at 200 °C. The Raman spectra of CNSs were taken using HORIBA Scientific Raman spectroscopy. The ζ potential values were measured using a Zetasizer Nano ZS90 obtained from Malvern Mastersizer.

Electrochemical Studies. The electrodes were made by mixing CNSs with 5 wt % polytetrafluoroethylene (PTFE) and 15 wt % carbon black. The electrochemical tests were performed using a two-electrode type system, in which the two electrodes were electrically isolated from each other by porous membrane in 5 M potassium hydroxide (KOH) electrolyte. The data were collected using an electrochemical workstation (Autolab/PGSTAT M101) equipped with a frequency response analyzer. Cyclic voltammetry tests were performed between 0 and 1 V with scan rates ranging from 2 to 100 mV s^{-1}. Charge−discharge galvanostatic tests were performed at current densities up to 1 A g^{-1}. Impedance data were collected from 500 kHz to 0.01 Hz, with 10 mV in ac amplitude signal at the open circuit potential (OCP).

ASSOCIATED CONTENT

Supporting Information

The Supporting Information is available free of charge on the ACS Publications website at DOI: 10.1021/acssuschemeng.5b00517.

TG-DTA curve of raw sago bark, TGA curve of nanoparticles, FESEM-EDX of CNSs, FTIR spectrum for CNSs, phase plot for CNSs (PDF)

AUTHOR INFORMATION

Corresponding Author

*E-mail: murthyhegde@gmail.com, hegde@bmsce.ac.in.

Author Contributions

H.G. contributed in designing, analyzing, and writing the manuscript. S.A. contributed in conducting experiments and also analyzing the experiments. G.A.M.A. and K.F.C. contributed in electrochemical studies of CNSs. K.A. contributed in characterizing and also writing the manuscript. Z.N. is responsible for measuring and characterization of TEM of the CNSs. K.V.S. is responsible for measuring and characterization of the Raman spectra of the CNSs.

Notes

The authors declare no competing financial interest.

ACKNOWLEDGMENTS

A.K. would like to acknowledge the European social fund within the framework of realizing the project "Support of intersectoral mobility and quality enhancement of research teams at Czech Technical University in Prague," CZ.1.07/2.3.00/30.0034.

ABBREVIATIONS

FESEM, Filed Emission Scanning Electron Microscopy; TEM, Transmission Electron Microscopy; XRD, X-ray Diffraction; PCN, Porous Carbon Nanospheres; BET, Brunauer−Emmett−Teller; FTIR, Fourier Transform Infrared; TGA, Thermo Gravimetric Analysis

REFERENCES

(1) Berger, C.; Song, Z.; Li, X.; Wu, X.; Brown, N.; Naud, C.; Mayou, D.; Li, T.; Hass, J.; Marchenkov, A. N.; Conrad, E. H.; First, P. N.; de Heer, W. A. Electronic confinement and coherence in patterned epitaxial graphene. *Science* **2006**, *312*, 1191.

(2) Gilje, S.; Han, S.; Wang, M.; Wang, K. L.; Kaner, R. B. A chemical route to graphene for device applications. *Nano Lett.* **2007**, *7* (11), 3394−3398.

(3) Guo, Y. G.; Hu, Y. S.; Maier, J. Synthesis of hierarchically mesoporous anatase spheres and their application in lithium batteries. *Chem. Commun.* **2006**, 2783−2785.

(4) Yuan, Z. Y.; Su, B. L. Insights into hierarchically meso-macroporous structured materials. *J. Mater. Chem.* **2006**, *16* (7), 663−677.

(5) Quercia, L.; Loffredo, F.; Alfano, B.; La Ferrara, V.; Di Francia, G. Fabrication and characterization of carbon nanoparticles for polymer based vapour sensors. *Sens. Actuators, B* **2004**, *100* (1), 22−28.

(6) Li, Y.; Fan, X.; Qi, J.; Ji, J.; Wang, S.; Zhang, G.; Zhang, F. Palladium nanoparticle-graphene hybrids as active catalysts for the Suzuki reaction. *Nano Res.* **2010**, *3* (6), 429−437.

(7) Lee, J.; Yoon, S.; Hyeon, T.; Oh, S.; Kim, K. Synthesis of a new mesoporous carbon and its application to electrochemical double-layer capacitors. *Chem. Commun.* **1999**, *21*, 2177−2178.

(8) Yang, H.; Shi, Q.; Liu, X.; Xie, S.; Jiang, D.; Zhang, F.; Yu, C.; Tu, B.; Zhao, D. Synthesis of ordered mesoporous carbon monoliths with bicontinuous cubic pore structure of Ia 3 d symmetry. *Chem. Commun.* **2002**, *23*, 2842−2843.

(9) Stoller, M. D.; Park, S.; Zhu, Y.; An, J.; Ruoff, R. S. Graphene-based ultracapacitors. *Nano Lett.* **2008**, *8* (10), 3498−3502.

(10) Thunga, M.; Chen, K.; Grewell, D.; Kessler, M. R. Bio-renewable precursor fibers from lignin/polylactide blends for conversion to carbon fibers. *Carbon* **2014**, *68*, 159−166.

(11) Golshadi, M.; Maita, J.; Lanza, D.; Zeiger, M.; Presser, V.; Schrlau, M. G. Effects of synthesis parameters on carbon nanotubes manufactured by template-based chemical vapor deposition. *Carbon* **2014**, *80*, 28−39.

(12) Pan, H.; Zang, J.; Li, X.; Wang, Y. One-pot synthesis of shell/core structural N-doped carbide-derived carbon/SiC particles as electrocatalysts for oxygen reduction reaction. *Carbon* **2014**, *69*, 630−633.

DOI: 10.1021/acssuschemeng.5b00517
ACS Sustainable Chem. Eng. 2015, 3, 2247−2253

(13) Miao, J. Y.; Hwang, D. W.; Narasimhulu, K. V.; Lin, P. I.; Chen, Y. T.; Lin, S. H.; Hwang, L. P. Synthesis and properties of carbon nanospheres grown by CVD using Kaolin supported transition metal catalysts. *Carbon* **2004**, *42* (4), 813−822.
(14) Wang, Z. L.; Kang, Z. C. Pairing of pentagonal and heptagonal carbon rings in the growth of nanosize carbon spheres synthesized by a mixed-valent oxide-catalytic carbonization process. *J. Phys. Chem.* **1996**, *100* (45), 17725−17731.
(15) Inagaki, M.; Kuroda, K.; Sakai, M. Pressure carbonization of polyethylene-polyvinylchloride mixtures. *Carbon* **1983**, *21* (3), 231−235.
(16) Yamada, K.; Tobisawa, S. Structure and formation process of carbon blacks formed by decomposing SiC powder using a conically converging shock-wave technique. *Carbon* **1989**, *27* (6), 845−852.
(17) Loa, I.; Moschel, C.; Reich, A.; Assenmacher, W.; Syassen, K.; Jansen, M. Novel graphitic spheres: Raman spectroscopy at high pressures. *Phys. Status Solidi B* **2001**, *223* (1), 293−298.
(18) Glerup, M.; Steinmetz, J.; Samaille, D.; Stephan, O.; Enouz, S.; Loiseau, A.; Roth, S.; Bernier, P. Synthesis of N-doped SWNT using the arc-discharge procedure. *Chem. Phys. Lett.* **2004**, *387* (1), 193−197.
(19) Zhang, Y.; Gu, H.; Suenaga, K.; Iijima, S. Heterogeneous growth of B□ C□ N nanotubes by laser ablation. *Chem. Phys. Lett.* **1997**, *279* (5), 264−269.
(20) De Jong, K. P.; Geus, J. W. Carbon nanofibers: catalytic synthesis and applications. *Catal. Rev.: Sci. Eng.* **2000**, *42* (4), 481−510.
(21) Subramanian, V.; Luo, C.; Stephan, A. M.; Nahm, K. S.; Thomas, S.; Wei, B. Supercapacitors from activated carbon derived from banana fibers. *J. Phys. Chem. C* **2007**, *111* (20), 7527−7531.
(22) Endo, M.; Kim, Y.; Osawa, K.; Ishii, K.; Inoue, T.; Nomura, T.; Miyashita, N.; Dresselhaus, M. S. High Capacitance EDLC Using a Carbon Material Obtained by Carbonization of PVDC The Effect of the Crystallite Size of the Pristine PVDC. *Electrochem. Solid-State Lett.* **2003**, *6* (2), A23−A26.
(23) Lv, G.; Wu, D.; Fu, R.; Zhang, Z.; Su, Z. Electrochemical properties of conductive filler/carbon aerogel composites as electrodes of supercapacitors. *J. Non-Cryst. Solids* **2008**, *354* (40), 4567−4571.
(24) Frackowiak, E.; Metenier, K.; Bertagna, V.; Beguin, F. Supercapacitor electrodes from multiwalled carbon nanotubes. *Appl. Phys. Lett.* **2000**, *77* (15), 2421−23.
(25) An, K. H.; Kim, W. S.; Park, Y. S.; Choi, Y. C.; Lee, S. M.; Chung, D. C.; Lee, Y. H. Supercapacitors using single-walled carbon nanotube electrodes. *Adv. Mater.* **2001**, *13* (7), 497−500.
(26) Kumar, A.; Hegde, G.; Abdul Manaf, S. A. B.; Ngaini, Z.; Sharma, K. V. Catalyst free silica templated porous carbon nanoparticles from bio-waste materials. *Chem. Commun.* **2014**, *50* (84), 12702−12705.
(27) Ali, G. A. M.; Abdul Manaf, S. A. B.; Kumar, A.; Chong, K. F.; Hegde, G. High performance supercapacitor using catalysis free porous carbon nanoparticles. *J. Phys. D: Appl. Phys.* **2014**, *47*, 495307−495312.
(28) Abdul Manaf, S. A. B.; Roy, P.; Sharma, K. V.; Ngaini, Z.; Malgras, V.; Aldalbahi, A.; Alshehri, S. M.; Yamauchi, Y.; Hegde, Gurumurthy Catalyst-free synthesis of carbon nanospheres for potential biomedical applications: waste to wealth approach. *RSC Adv.* **2015**, *5*, 24528−24533.
(29) Gao, W.; Singh, N.; Song, Li.; Liu, Z.; Reddy, A. L. M.; Ci, L.; Vajtai, R.; Zhang, Q.; Wei, B.; Ajayan, P. M. Direct laser writing of micro-supercapacitors on hydrated graphite oxide films. *Nat. Nanotechnol.* **2011**, *6*, 496−500.
(30) Sun, R. C.; Jones, G. L.; Tomkinson, J.; Bolton, J. Fractional isolation and partial characterization of non-starch polysaccharides and lignin from sago pith. *Ind. Crops Prod.* **1999**, *9* (3), 211−220.
(31) Sim, S. F.; Mohamed, M.; Lu, N.A.L.M.I.; Sarman, N. S. P.; Samsudin, S. N. S. Computer-assisted analysis of Fourier Transform Infrared (FTIR) spectra for characterization of various treated and untreated agriculture biomass. *BioResources* **2012**, *7* (4), 5367−5380.
(32) Cheng, C. H.; Lehmann, J.; Thies, J. E.; Burton, S. D.; Engelhard, M. H. Oxidation of black carbon by biotic and abiotic processes. *Org. Geochem.* **2006**, *37* (11), 1477−1488.
(33) Peng, F.; Ren, J. L.; Xu, F.; Bian, J.; Peng, P.; Sun, R. C. Comparative study of hemicelluloses obtained by graded ethanol precipitation from sugarcane bagasse. *J. Agric. Food Chem.* **2009**, *57* (14), 6305−6317.
(34) Kacurakova, M.; Capek, P.; Sasinkova, V.; Wellner, N.; Ebringerova, A. FT-IR study of plant cell wall model compounds: pectic polysaccharides and hemicelluloses. *Carbohydr. Polym.* **2000**, *43* (2), 195−203.
(35) Mathew, A. P.; Oksman, K.; Sain, M. Mechanical properties of biodegradable composites from poly lactic acid (PLA) and microcrystalline cellulose (MCC). *J. Appl. Polym. Sci.* **2005**, *97* (5), 2014−2025.
(36) Li, Z.; Wu, D.; Liang, Y.; Xu, F.; Fu, R. Facile fabrication of novel highly microporous carbons with superior size-selective adsorption and supercapacitance properties. *Nanoscale* **2013**, *5* (22), 10824−10828.
(37) Kuga, S.; Kim, D.-Y.; Nishiyama, Y.; Brown, R. M. Nanofibrillar carbon from native cellulose. *Mol. Cryst. Liq. Cryst.* **2002**, *387* (1), 13−19.
(38) Wu, Z.-Y.; Li, C.; Liang, H.-W.; Chen, J.-F.; Yu, S.-H. Ultralight, Flexible, and Fire-Resistant Carbon Nanofiber Aerogels from Bacterial Cellulose. *Angew. Chem., Int. Ed.* **2013**, *52* (10), 2925−2929.
(39) Klemm, D.; Heublein, B.; Fink, H.-P.; Bohn, A. Cellulose: fascinating biopolymer and sustainable raw material. *Angew. Chem., Int. Ed.* **2005**, *44* (22), 3358−3393.
(40) Li, Y.; Chen, J.; Xu, Q.; He, L.; Chen, Z. Controllable route to solid and hollow monodisperse carbon nanospheres. *J. Phys. Chem. C* **2009**, *113* (23), 10085−10089.
(41) Li, Y.; Lee, E. J.; Cai, W. P.; Kim, K. Y.; Cho, S. O. Unconventional method for morphology-controlled carbonaceous nanoarrays based on electron irradiation of a polystyrene colloidal monolayer. *ACS Nano* **2008**, *2* (6), 1108−1112.
(42) Qian, H. S.; Han, F. M.; Zhang, B.; Guo, Y. C.; Yue, J.; Peng, B. X. Non-catalytic CVD preparation of carbon spheres with a specific size. *Carbon* **2004**, *42* (4), 761−766.
(43) Miao, J. Y.; Hwang, D. W.; Narasimhulu, K. V.; Lin, P. I.; Chen, Y. T.; Lin, S. H.; Hwang, L. P. Synthesis and properties of carbon nanospheres grown by CVD using Kaolin supported transition metal catalysts. *Carbon* **2004**, *42* (4), 813−822.
(44) White, B.; Banerjee, S.; O'Brien, S.; Turro, N. J.; Herman, P. I. Zeta-potential measurements of surfactant-wrapped individual single-walled carbon nanotubes. *J. Phys. Chem. C* **2007**, *111* (37), 13684−13690.
(45) Liu, C.; Yu, Z.; Neff, D.; Zhamu, A.; Jang, B. Z. Graphene-based supercapacitor with an ultrahigh energy density. *Nano Lett.* **2010**, *10* (12), 4863−4868.
(46) Kleszyk, P.; Ratajczak, P.; Skowron, P.; Jagiello, J.; Abbas, Q.; Frackowiak, E.; Béguin, F. Carbons with narrow pore size distribution prepared by simultaneous carbonization and self-activation of tobacco stems and their application to supercapacitors. *Carbon* **2015**, *81*, 148−157.

DOI: 10.1021/acssuschemeng.5b00517
ACS Sustainable Chem. Eng. 2015, 3, 2247−2253